SO_4^* complex in CdTe: Infrared absorption spectroscopy and first-principles calculations

F. Herklotz* and E. V. Lavrov
Technische Universität Dresden, 01062 Dresden, Germany

Vladlen V. Melnikov
Tomsk State University, 634050 Tomsk, Russia

(Received 11 May 2021; accepted 8 July 2021; published 19 July 2021)

A sulfur-oxygen complex in CdTe characterized by IR absorption lines at 1097 and 1108 cm^{-1} is studied by means of infrared absorption spectroscopy and first principles theory. Temperature-sensitive measurements performed on samples with different ^{16}O:^{18}O isotope ratios show that these lines are due to a split ν_3 stretch vibrational mode of a disturbed sulfate ion (SO_4^{2-}) transformed under the A_1 (1097 cm^{-1}) and E (1108 cm^{-1}) representations of the C_{3v} point group. The ν_1 symmetric stretch, ν_4 bend, and $\nu_1 + \nu_3$ combination modes of the ion are also identified. An axially disturbed SO_4 located at the Cd vacancy site is proposed as a microscopic model of the complex.

DOI: 10.1103/PhysRevB.104.035204

I. INTRODUCTION

Over the last decades, CdTe has spurred an immense research interest as a key material for several high-efficiency applications including room temperature pixel X-ray, γ-ray, α-particle, and β-particle detectors [1–3] as well as thin-film photovoltaics [4,5]. Impurities and their complexes with native defects play an important role in the performance of all semiconductor devices. Particular examples of relevance for the present study are oxygen and sulfur in CdTe thin-film solar cells.

Oxygen may be introduced into CdTe during multiple steps of the solar cell fabrication process, for instance, from an ambient during CdTe deposition, at the post-growth chloride "activation" process, in-diffused from CdS:O window layers, or from an oxygen-rich back contact. While its presence proved to be strongly beneficial for grain boundary nucleation and passivation as well as intermixing of CdTe with CdS window layers [6–8], oxygen-related defects may also have a detrimental influence as carrier recombination centers [9,10]. Sulfur, on the other hand, out-diffuses from CdS and adds to the well established phenomenon of Cd-S-Te intermixing at the CdS/CdTe interface. There is increasing evidence that an interaction of S and O impurities in this CdS_xTe_{1-x} interface region hinders the intermixing process [11–13]. The cumulative impact of both elements, oxygen and sulfur, on CdTe solar cell performance, however, is unclear without conclusive understanding of the fundamental properties of these impurities and their complexes in the CdTe host material.

The subject of the present work is a sulfur-oxygen complex in single-crystalline CdTe, hereafter labeled as SO_n^*, which results in a doublet feature of local vibrational modes (LVMs) at about 1097 and 1108 cm^{-1} [14–16]. While the involvement of sulfur and oxygen in SO_n^* was convincingly evidenced by the spectroscopic identification of weak ^{34}S isotope analogs of the main ^{32}S features [16] and in-growth oxygen doping experiments [14,15], the microscopic structure of the complex remains unidentified. The original model of a SO_2^* molecule [16] turned out to be not fully consistent with recent results of first principles calculations [17].

In this work, we present results of first principles calculations and IR absorption measurements on CdTe single crystals codoped with ^{16}O and ^{18}O isotopes. We will show that the vibrational spectrum of SO_n^* is consistent with an axially distorted tetragonal SO_4^{2-} sulfate ion occupying the cadmium site of the CdTe host.

II. METHODS

A. Experimental details

For this study we used (100)-oriented CdTe single crystals grown via the traveling heater method at the Freiburger Materialforschungszentrum, Germany.

Fourier transform infrared (FTIR) absorbance spectra were recorded with a Bomem DA3.01 Fourier transform spectrometer equipped with a Globar light source, a KBr beam splitter, and a liquid nitrogen cooled mercury cadmium telluride (MCT) detector. The measurements were performed in a He exchange-gas cryostat, with the temperature of the samples stabilized within 1 K in the range of 7–180 K. The spectral resolution was 0.1–0.5 cm^{-1}. Polarized light was produced by a wire grid polarizer with a KRS-5 substrate. Unless noted otherwise, measurements were taken at ∼10 K with the wave vector $\boldsymbol{k}$ of unpolarized light directed along the [100] axis of the CdTe samples.

In order to generate the defects of interest, the samples were subjected to one of the two following treatments. In the first, labeled as "$CdSO_4$ treatment," the samples were sealed in quartz ampules filled with 16 mg $CdSO_4$ powder and 250 mbar argon gas, and subjected to thermal treatments at 850 °C for 60–315 min. Such treatments introduces SO_n^* in CdTe with

*frank.herklotz1@tu-dresden.de

natural abundances of oxygen isotopes. In the second, labeled as "($CdS + O_2$) treatment," samples were sealed in quartz ampules filled with ~3 mg CdS powder and 400 mbar oxygen gas, and subjected to thermal treatments at 850 °C for 1 h. For this doping procedure the ^{16}O:^{18}O ratio could be varied by the different ^{18}O enrichment of the oxygen ambient.

B. Computational details

The calculations of the local structure and vibrational properties of defects under consideration were carried out within the framework of the density functional theory (DFT) using the projector augmented wave (PAW) method [18] and the local density approximation (LDA) to the exchange-correlation energy functional as implemented in ABINIT code [19,20]. Under the theoretical approach chosen an estimated lattice constant of bulk CdTe with the zinc-blende crystal structure, $a = 6.42$ Å, is in good agreement with the corresponding experimental value of 6.46 Å [21].

To construct the defect models a $2a \times 2a \times 2a$ cubic supercell with the periodic boundary conditions initially comprising 32 formula units was employed. The necessary number of impurity atoms was added, and a Cd vacancy was created by removing an appropriate atom.

Series of high precision structure optimizations and subsequent calculations were performed using the $2 \times 2 \times 2$ grid of k points and the energy cutoff of 40 hartree for the plane wave basis set. In doing so the energy cutoff for the fine FFT grid definition was set to 50 hartree. Corresponding phonon modes at the Γ point were calculated using the density-functional perturbation theory, [22–24] wherein all possible displacements of S and O atoms were taken into account.

III. MICROSCOPIC MODEL AND CALCULATIONS

In the following sections we will give strong evidence that the SO_n^* complex is an axially distorted tetragonal SO_4^{2-} sulfate ion occupying the cadmium site of the regular CdTe lattice. The vibrational spectrum of a free SO_4^{2-} consists of four fundamental modes transformed under the $A_1 + E + 2T_2$ irreducible representations of the T_d point group. The corresponding frequencies given by Herzberg are $\nu_2(E) = 451$ cm^{-1}, $\nu_4(T_2) = 613$ cm^{-1}, $\nu_1(A_1) = 981$ cm^{-1}, and $\nu_3(T_2) = 1104$ cm^{-1} [25]. The ν_1 and ν_2 modes are infrared inactive, whereas each of the triply degenerate ν_3 and ν_4 modes gives rise to a strong IR absorption band.

Note that the 1097 and 1108 cm^{-1} IR absorption lines considered in Refs. [14–16] were referred to as ν_1 and ν_2, respectively. These notations, however, do not correspond to those given by Herzberg for the SO_4^{2-} ion. To avoid confusion with the earlier works, we will relabel the 1097 and 1108 cm^{-1} lines as ϑ_1 and ϑ_2, respectively.

In order to identify possible structures of the SO_n^* complex we performed series of *ab initio* calculations for the CdTe crystal containing a SO_n moiety ($n = 1, 2, 3, 4$) as an interstitial impurity, and a substitutional impurity located at the Cd vacancy site.

Validation of the defect structure was carried out in conjunction with available experimental data based on the local symmetry and vibrational modes of test complexes.

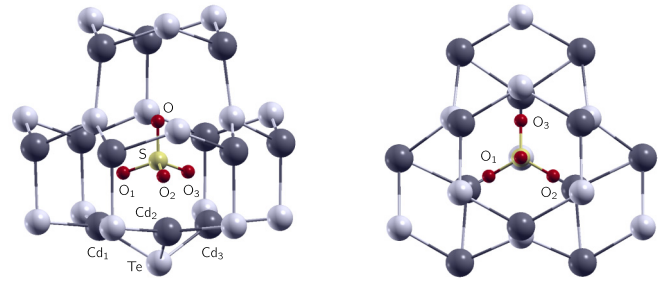

FIG. 1. Calculated structure of the SO_4–V_{Cd} complex in CdTe: left, general view; right, view along the ⟨111⟩ direction. Cd, Te, S, and O atoms are light gray, dark gray, yellow, and red, respectively. The local symmetry of the defect is C_{3v}. The S–O bond is aligned along the ⟨111⟩ direction. Each of the mirror σ_i planes ($i = 1, 2, 3$) passes correspondingly through the O, S, O_i, Cd_i, and Te atoms labeled in the figure.

Among all trial structures, the only configuration consistent with the experiment was found to be the SO_4 ion enclosed inside the Cd vacancy (SO_4–V_{Cd}). We found that a T_d configuration in which the sulfur atom is positioned at the vacancy center and four identical S–O bonds are oriented along the corresponding ⟨111⟩ directions is unstable. Instead, the SO_4–V_{Cd} complex possesses four equivalent equilibrium geometries of C_{3v} symmetry with the S atom being slightly shifted along one of the ⟨111⟩ directions.

Figure 1 shows a calculated structure of the SO_4–V_{Cd} complex in CdTe. A general view and view along the ⟨111⟩ direction are given. The S–O bond is aligned along the ⟨111⟩ direction. Each of the mirror σ_i planes ($i = 1, 2, 3$) passes correspondingly through the O, S, O_i, Cd_i, and Te atoms as labeled in the figure. The S atom is displaced from the vacancy center by about 0.5 Å towards the next Te atom along ⟨111⟩. In turn, this Te atom leaves the corresponding {111} plane moving outside the vacancy approximately by 1.3 Å (see labeled atoms in Fig. 1). Calculated S–O and S–O_i bond lengths are about 1.48 and 1.49 Å, respectively. The angle $\angle OSO_i$ is 108.7°, i.e., close to the value of 109.5° corresponding to the tetrahedral molecular geometry. The distance between O_i and Cd_i atoms is about 2.2 Å.

Reduction of the cubic symmetry of the SO_4^{2-} ion from T_d to C_{3v} results in the splitting of the T_2 vibrational modes into a nondegenerate A_1 and twofold degenerate E mode. The calculated values of the vibrational frequencies for the most abundant isotope configuration of SO_4–V_{Cd} are listed in Table I, wherein the A_1 and E split modes of the two T_2 representations are labeled as ν' and ν'', respectively. Experimental frequencies of the free tetrahedral sulfate ion are given for comparison. Taking into account that the ϑ_2 line at 1108 cm^{-1} is approximately twice as strong as the ϑ_1 one at 1097 cm^{-1} [14–16], these modes should be assigned to the E and A_1 representations of the C_{3v} point group, respectively. Note that splitting of the ν_3 mode due to the reduced symmetry has been reported previously for sulfate ions trapped in various hosts (see, e.g., Ref. [26]).

It follows from the table that the calculated frequencies of the A_1 (ν_3') and E (ν_3'') modes as well as the magnitude and order of the A_1-E splitting of the SO_4–V_{Cd} complex are in good

TABLE I. Calculated vibrational modes (cm^{-1}) of the SO_4–V_{Cd} complex in CdTe and those observed for free tetrahedral sulfate ion SO_4^{2-} (see Ref. [25]).

SO_4^{2-}			SO_4–V_{Cd}		
451	ν_2	E	418	ν_2	E
613	ν_4	T_2	545	ν_4'	A_1
			568	ν_4''	E
981	ν_1	A_1	940	ν_1	A_1
1104	ν_3	T_2	1010	ν_3'	A_1
			1014	ν_3''	E

agreement with the experimental data. This finding supports the sulfate ion model of the SO_n^* complex. In the following sections, we will present further experimental evidences for the validity of this model obtained from the spectral range of ν_3, ν_1, ν_4, and combinational $\nu_3 + \nu_1$ modes.

IV. EXPERIMENTAL RESULTS

A. The ν_3 stretch modes

Figure 2 shows IR absorbance spectra obtained for (CdS + O_2)-treated CdTe samples. The spectra are normalized to the absorbance integrated over the spectral range 1060–1110 cm^{-1}. The top spectrum has been recorded on a sample treated with natural oxygen gas (0.2% of ^{18}O), whereas for the midle and bottom spectra the amount of ^{18}O in the oxygen ambient was 50 and 97%, respectively. All features seen in the figure were observed only as a result of the treatments. In the case of natural oxygen, the two previously reported modes ϑ_1 (1097 cm^{-1}) and ϑ_2 (1108 cm^{-1}) due to the SO_n^* complex dominate the spectrum [14–16]. Weaker lines at about 1083 and 1094 cm^{-1} result from isotopic ^{34}S counterparts of ϑ_1 and ϑ_2, respectively [16].

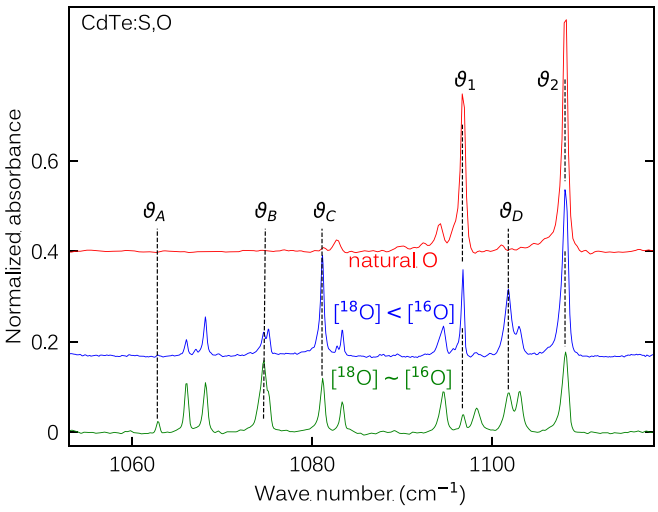

FIG. 2. Infrared absorption spectra obtained for (CdS + O_2)-treated CdTe samples with different ^{18}O:^{16}O ratios of the oxygen ambient: top, natural abundances; middle, ^{18}O:^{16}O = 1 : 1; bottom, ^{18}O:^{16}O = 97 : 3. Spectra are vertically offset for clarity and normalized to the integrated absorbance in the range 1060–1110 cm^{-1}.

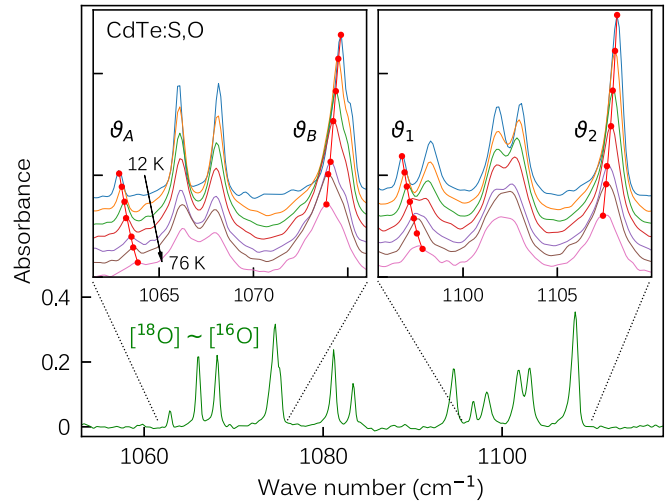

FIG. 3. Temperature-dependent IR absorption spectra recorded for a (CdS + O_2)-treated CdTe sample annealed in the ^{18}O:^{16}O = 97 : 3 ambient. Spectra given in the inserts are vertically offset for clarity.

As can be seen from the lower two spectra, the ^{18}O-enriched CdTe samples reveal a number of new IR absorption lines. Altogether, at least 13 different modes occur in the 1060–1110 cm^{-1} range. Moreover, the different oxygen isotope ambients also result in distinct redistributions of the vibrational mode intensities. In particular, the intensity ratio of the ϑ_1 and ϑ_2 modes significantly decreases as the ^{18}O:^{16}O ratio grows in. These results disagree with the sulfur-dioxygen model (SO_2^*) proposed earlier for the defect under study [16], strongly indicating that the SO_n^* complex includes more than two oxygen atoms.

We emphasize that whereas the isotopic ^{18}O:^{16}O ratio of the gas ambient was varied for each of the (CdS + O_2) treatments presented in the figure, the actual amount of ^{18}O introduced into the samples could not be controlled. It turned out that an unintentional source of natural oxygen—resulting, most likely, from outgassing during fusion sealing of the quartz ampules—enhanced the amount of ^{16}O in the gas ambient. As a result, the actual ^{18}O:^{16}O ratio in the samples was significantly lower than expected. In fact, even the nominally pure ^{18}O ambient during the treatment resulted in only ^{18}O:^{16}O = 1:1 ratio.

In order to unveil the complete vibrational spectrum of SO_n^*, we first focus on the identification of IR absorption lines resulting from $^{32}S\,^{18}O_n^*$. This complex should give rise to two distinct features "redshifted" relative to the ϑ_1 and ϑ_2 modes of its isotopic ^{16}O counterpart.

Figure 3 shows temperature dependent spectra of a (CdS + O_2)-treated CdTe sample annealed in the ^{18}O:^{16}O = 97 : 3 ambient. As can be seen from the right insert, the ϑ_1 and ϑ_2 modes due to $^{32}S\,^{16}O_n^*$ "blue" and "red" shift, respectively, with the temperature. Importantly, two lines at 1062.9 and 1074.6 cm^{-1}, denoted as ϑ_A and ϑ_B (left insert), display a strikingly similar temperature dependence, both in sign and magnitude of the frequency shifts. The difference in frequency of these lines at ~10 K, 1074.6 − 1062.9 = 11.7 cm^{-1}, is very close to that of the ϑ_1 and ϑ_2 modes, 1108.4−1096.8 =

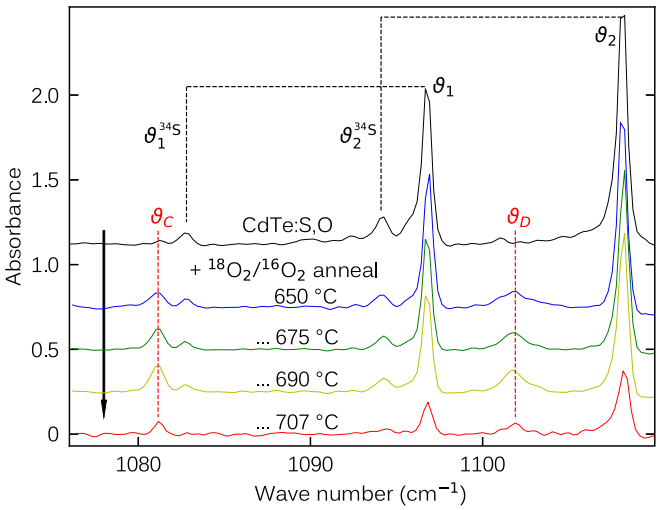

FIG. 4. IR absorption spectra obtained for a $CdSO_4$-treated CdTe sample which has been subsequently subjected to a series of thermal treatments (30 min) in ^{18}O-enriched oxygen ambient. Spectra are vertically offset for clarity.

11.6 cm^{-1}. Moreover, the ϑ_A mode has the lowest frequency of all features observed in the spectra and becomes visible only in the sample with the highest ^{18}O content. Based on these observations, we attribute ϑ_A and ϑ_B to the ^{32}S $^{18}O_n^*$ counterparts of ϑ_1 and ϑ_2.

We now turn to a $CdSO_4$-treated CdTe sample, with natural oxygen isotope abundances, subsequently subjected to a series of thermal treatments in ^{18}O-enriched oxygen ambient. The results are shown in Fig. 4. The as-treated sample (upper spectrum) shows strong ϑ_1 and ϑ_2 signals together with their weaker isotopic ^{34}S counterparts at about 1083 and 1094 cm^{-1}. No features due to ^{18}O can be spotted. Subsequent annealing in oxygen atmosphere with equal content of ^{18}O and ^{16}O at 650 °C for 30 min (blue spectrum), however, gives rise to two additional lines at 1081 cm^{-1} (ϑ_C) and 1101.7 cm^{-1} (ϑ_D). The features gain further in intensity after annealings at 675 and 690 °C (green and yellow spectrum). We tentatively attribute these modes to SO_n^* complexes in which one ^{16}O atom has been replaced by ^{18}O in the cause of oxygen in-diffusion. Further annealing at 707 °C (red spectrum) results in a significant reduction of all IR absorption lines, most likely due to dissociation of SO_n^*.

In order to unveil the nature of all IR absorption lines occurring in the spectra presented in Fig. 2 we have to turn to the SO_4–V_{Cd} model of SO_n^* put forward in Sec. III. Vibrational stretch mode frequencies of a distorted tetrahedral SO_4 complex of C_{3v} symmetry can be obtained in the valence force approximation from the solution of the secular equation [27]

$$\|\hat{\boldsymbol{F}}\hat{\boldsymbol{G}} - \omega^2\hat{\boldsymbol{E}}\| = 0, \tag{1}$$

with the identity matrix $\hat{\boldsymbol{E}}$ and matrices

$$\hat{\boldsymbol{F}} = \begin{pmatrix} F_\parallel & f' & f' & f' \\ f' & F_\perp & f'' & f'' \\ f' & f'' & F_\perp & f'' \\ f' & f'' & f'' & F_\perp \end{pmatrix}, \tag{2}$$

TABLE II. Calculated stretch vibrational modes (cm^{-1}) of an axially distorted tetrahedral SO_4 complex (see text for further details) together with experimentally observed LVMs of the SO_n^* center. Notations *a* and *b* stand for the axial and basal orientation of the corresponding S–O bond relative to the trigonal axis of the defect, respectively. The last column denotes the sign of the frequency shift with the temperature.

Configuration							
a	*b*	*b*	*b*	Label	ω_{exp}	ω_{calc}	ω_{diff}	$\Delta\omega(T)$
^{16}O	^{16}O	^{16}O	^{16}O	ϑ_1	1096.8	1097.2	0.4	+
				ϑ_2	1108.4	1108.6	0.2	–
^{18}O	^{16}O	^{16}O	^{16}O	ϑ_C	1081.1	1081.4	0.3	–
				ϑ_2	1108.4	1108.6	0.2	–
^{16}O	^{18}O	^{16}O	^{16}O	ϑ_C	1080.8	1080.9	0.1	–
				ϑ_D	1101.8	1100.7	−1.1	–
				ϑ_2	1108.4	1108.6	0.2	–
^{18}O	^{18}O	^{16}O	^{16}O	–	1068.1	1068.1	0.0	–
				–	1094.6	1094.6	0.0	–
				ϑ_2	1108.4	1108.6	0.2	–
^{16}O	^{18}O	^{18}O	^{16}O	ϑ_B	1075.2	1075.3	0.1	–
				–	1083.3	1084.2	0.9	–
				–	1103.3	1104.5	1.2	–
^{18}O	^{18}O	^{18}O	^{16}O	–	1066.0	1065.7	−0.3	+
				ϑ_B	1074.6	1075.3	0.7	–
				–	1098.4	1102.4	4.0	–
^{16}O	^{18}O	^{18}O	^{18}O	ϑ_B	1074.6	1075.3	−0.7	–
				–	1087.1	1086.1	−1.0	–
^{18}O	^{18}O	^{18}O	^{18}O	ϑ_A	1062.9	1063.1	0.2	+
				ϑ_B	1074.6	1075.3	0.7	–

$$\hat{\boldsymbol{G}} = \begin{pmatrix} 1/\mu & \cos\varphi/m_S & \cos\varphi/m_S & \cos\varphi/m_S \\ \cos\varphi/m_S & 1/\mu & \cos\varphi/m_S & \cos\varphi/m_S \\ \cos\varphi/m_S & \cos\varphi/m_S & 1/\mu & \cos\varphi/m_S \\ \cos\varphi/m_S & \cos\varphi/m_S & \cos\varphi/m_S & 1/\mu \end{pmatrix}. \tag{3}$$

Here, $1/\mu = 1/m_S + 1/m_O$ is the reduced mass of the S–O bond with $m_S = 32$ a.u. and m_O equals 16 or 18 a.u.; $F_\parallel$ and $F_\perp$ are the force constant of the S–O bonds with axial and basal orientation relative to the trigonal symmetry axis of the defect, respectively; f' and f'' are interaction force constants; φ is the O–S–O angle which for simplicity—as also supported by the first principles calculations presented in Sec. III—we assumed to be tetragonal ($\varphi = 109.5°$). The influence of bending modes is neglected.

Table II gathers the "best-fit" frequencies of the axially distorted SO_4^* complex together with the local vibrational modes of different isotopic configurations of SO_n^* shown in Fig. 2. As one can see, the calculated frequencies agree quite well with experiment thus providing unambiguous assignments of all experimentally observed IR absorption lines to distinct isotopic varieties of SO_4^*.

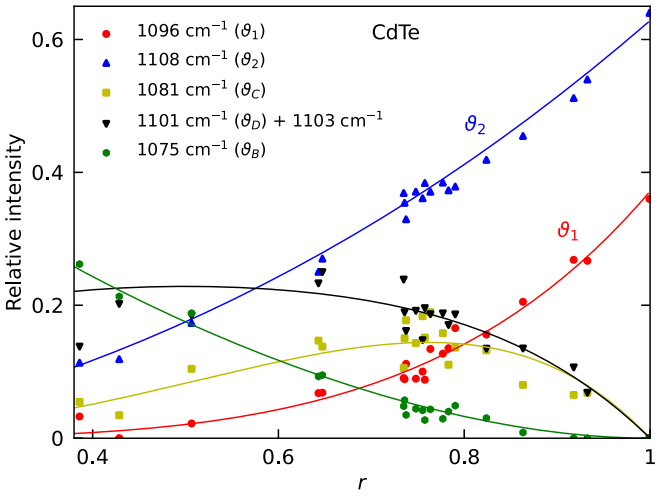

FIG. 5. Best fit of relative LVM intensities of different isotopic configurations due the SO_n^* center obtained on the basis of the SO_4^* model (see text for details). The relative ^{16}O content, $r = [^{16}O]/([^{16}O] + [^{18}O])$, was treated as a fitting parameter and was varied independently for each sample to give the best fit to all data.

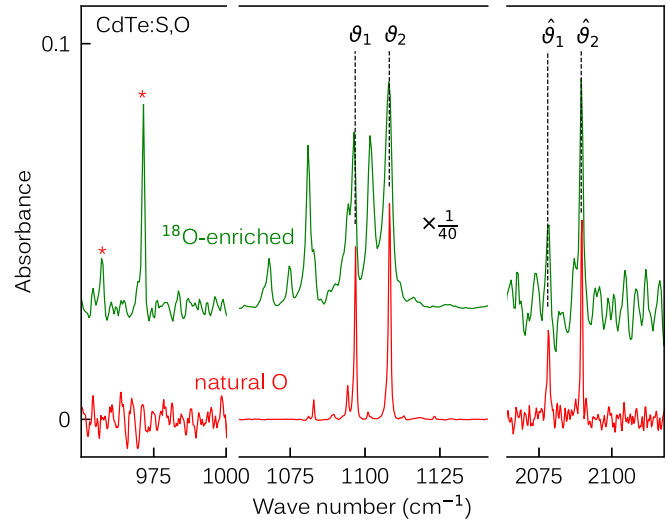

FIG. 6. IR absorption spectra obtained for $CdSO_4$-treated (bottom) and ($CdS + O_2$)-treated CdTe samples with the ^{18}O:$^{16}O = 1:1$ isotope ratio of the gas ambient (top).

Further support of the SO_4^* model comes from the relative intensities of the IR absorption lines. As mentioned above, the actual ^{18}O:^{16}O ratio of the oxygen isotopes introduced into CdTe samples significantly deviated from that of the gas ambient during the thermal treatment. Because of this, the absolute intensity of each isotope-specific LVM of SO_n^* in the IR absorption spectra varied from sample to sample. However, the *relative* LVM intensities within each isotopic configuration should depend solely on the the isotopic ratio $r = [^{16}O]/([^{16}O] + [^{18}O])$.

Assuming that the incorporation of ^{16}O and ^{18}O on a certain position in the SO_4^* tetrahedron is governed by random statistics, the relative intensities of each mode can be easily estimated. For example, LVMs of S $^{16}O_4^*$ and S $^{18}O_4^*$ should occur in the spectra with the probabilities of r^4 and $(1-r)^4$, respectively. The configuration with a single ^{18}O atom would consist of two groups of modes differing by the orientation of the S–^{18}O bond relative to the trigonal axis of the defect, whereby the axial and basal configurations occur with the probabilities of $(1-r)r^3$ and $3(1-r)r^3$, respectively. In a similar manner, the relative intensities for all isotopic configurations of the SO_4^* complex can be constructed and compared against the experimental data.

Figure 5 shows the relative intensities of the most prominent IR absorption lines of the SO_n^* complex together with the best-fit curves as a function of r obtained for 20 CdTe samples subjected to different isotopic ^{18}O - ^{16}O treatments. Since the value of r was not known *a priori*, it was treated as a fitting parameter. For simplicity we also assumed that the absorption strength of each mode is equal to the mean value of the ϑ_1 and ϑ_2 modes. As follows from the figure, our model accounts for the experimental data reasonably well. We take these observations as further support for the consistency of the tetrahedron SO_4^* model.

B. The ν_1 symmetric stretch and $\nu_1 + \nu_3$ combination modes

Figure 6 shows expanded IR absorption spectra obtained for two CdTe samples subjected to different SO_n^* doping procedures. The lower spectrum was obtained after a $CdSO_4$ treatment, inherently displaying natural abundances of oxygen isotopes. The upper spectrum was recorded on a ($CdS + O_2$)-treated CdTe sample for which the oxygen atmosphere was ^{18}O enriched.

In both cases the ν_3 stretch modes of SO_n^* at about 1060–1110 cm^{-1} dominate the spectra (note the scaling factor of $\times\frac{1}{40}$ for this spectral range). In addition to these lines, a number of significantly weaker features are also seen in the figure. We first turn our focus to two previously unreported lines at 957 and 971 cm^{-1} marked by a red star. As follows from Table I, these modes match that of the symmetric stretching mode $\nu_1(A_1)$ of SO_4–V_{Cd}. In the case of the cubic symmetry of free SO_4^{2-}, the ν_1 mode is forbidden in IR absorption but might become visible for the distorted SO_4–V_{Cd} complex. The bottom spectrum in Fig. 6 recorded for the sample with the natural abundances of oxygen isotopes, however, indicates that the trigonal distortion of the sulfate ion is insufficient to detect the corresponding transition of S $^{16}O_4^*$.

The situation changes for the ^{18}O-enriched CdTe sample ($r = 0.74$) whose spectrum is also presented in Fig. 6. For such an enrichment the expected occurrences of SO_4^* with the ^{18}O:^{16}O isotope ratios of 0:4, 1:3, 2:2, 3:1, and 4:0 are 0.30, 0.42, 0.22, 0.05, and 0.005, respectively. That is, the complex with a single ^{18}O isotope has the maximum occurrence, whereby the basal orientation of the S–^{18}O bond is thrice as probable compared to the axial one.

We propose, therefore, that the 971- and 957-cm^{-1} lines are due to the ν_1-like modes of the SO_4^* complex comprising a single ^{32}S–^{18}O bond of the basal and axial orientation, respectively. Indeed, the distortion of SO_4^* caused by the replacement of an ^{16}O atom with a heavier isotope should contribute much more to the IR activity of the ν_1-like mode compared to the trigonal deformation of SO_4^{2-}.

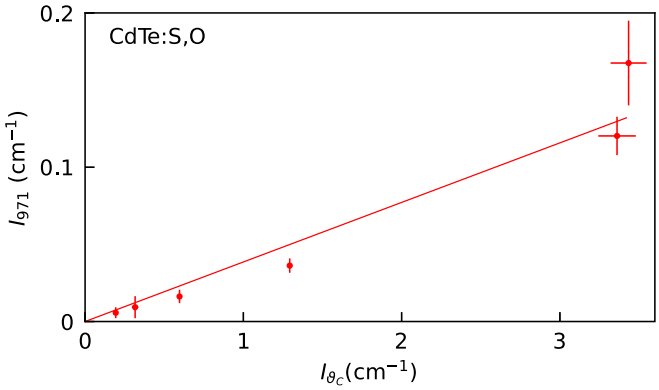

FIG. 7. Integrated intensity of the ϑ_C mode at 1081 cm^{-1} as a function of that at 971 cm^{-1} obtained from a set of ^{18}O-enriched CdTe samples.

Further support of our assignment comes from the intensity correlation of the 971-cm^{-1} and the ϑ_C (1081-cm^{-1}) lines given in Fig. 7. The SO_4^* model assigns both modes to the isotopic configuration with a single ^{32}S–^{18}O bond of the basal orientation relative to the trigonal axis of the defect (see Table II). Evidently, the intensity of the 971-cm^{-1} feature scales linearly with that of ϑ_C, which we take as a further indication for the validity of our model.

We now turn to the spectral range 2070–2110 cm^{-1} in Fig. 6. Two lines at about 2078 ($\hat{\vartheta}_1$) and 2089 cm^{-1} ($\hat{\vartheta}_2$) appear in the spectra of CdTe which were previously interpreted as first overtones of the ϑ_1 and ϑ_2 fundamentals [16]. Our results presented this far strongly suggest that these lines should be reassigned to $\nu_1 + \nu_3$ combination modes of SO_4^*. Notably, the frequency differences of each pair of lines, i.e., $\hat{\vartheta}_1$ vs ϑ_1 and $\hat{\vartheta}_2$ vs ϑ_2, are equal to 981 cm^{-1}, i.e. that of the ν_1 mode due to free SO_4^{2-} (see Table I).

Frequency shifts of the ϑ_1, ϑ_2, $\hat{\vartheta}_1$, and $\hat{\vartheta}_2$ lines with the temperature presented in Fig. 8 strengthen our interpretation even further. The left panel in the figure shows the shifts relative to the values obtained at 10 K. Both pairs of lines show a strikingly similar "merging" behavior; that is, the low-frequency modes "blue" shift whereas the high-frequency

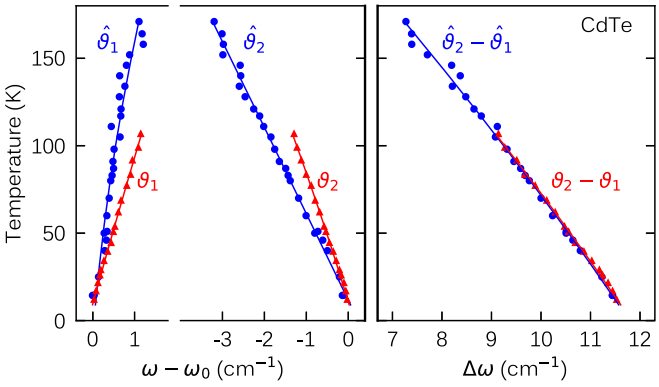

FIG. 8. Temperature-dependent frequency shifts (left panel) and differences in frequency (right panel) of the ϑ_1 and ϑ_2 modes (red) as well as those of the $\hat{\vartheta}_1$ and $\hat{\vartheta}_2$ modes (blue) obtained for a $CdSO_4$-treated CdTe sample.

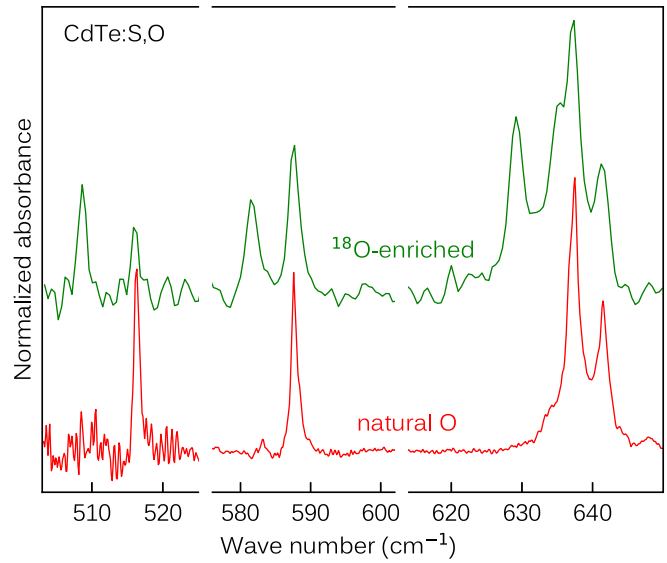

FIG. 9. IR absorption spectra obtained for $CdSO_4$- (bottom) and ($CdS + O_2$)-treated CdTe samples with the ^{18}O:$^{16}O = 1:1$ isotope ratio of the gas ambient (top). Spectra are normalized to their peak absorbance in the spectral range 637 ± 3 cm^{-1}.

ones "red" shift with the temperature. More importantly, the differences in frequency between each pair of lines are equal to each other, as seen from the right panel in Fig. 8. The finding is naturally explained if $\hat{\vartheta}_1$ and $\hat{\vartheta}_2$ are combinational modes since in this case

$$\omega_{\vartheta_2} - \omega_{\vartheta_1} = (\omega_{\vartheta_2} + \omega_{\nu_1}) - (\omega_{\vartheta_1} + \omega_{\nu_1}) = \omega_{\hat{\vartheta}_2} - \omega_{\hat{\vartheta}_1}.$$

C. The ν_4 bending modes

Finally we consider the spectral range where bending modes of the SO_4^* units are expected to occur. Figure 9 shows IR absorption spectra obtained for two CdTe samples subjected to SO_n^* doping procedures, similar to those presented in Fig. 6. The sample with natural oxygen isotope abundances reveals two single modes at about 517 and 588 cm^{-1} as well as a double feature at about 640 cm^{-1}. The substructure of additional lines appearing in the ^{18}O-enriched CdTe sample indicates that all these signals are also related to complexes containing oxygen. The entirety of our experimental data shows that the intensities of the 588- and 640-cm^{-1} features scale linearly with those of the ν_3-like stretch modes of SO_4^* at about 1100 cm^{-1}. Due to substantial noise in the spectra of ^{18}O-enriched samples we can neither confirm nor rule out a similar correlation for the 517-cm^{-1} line.

We tentatively assign the 640-cm^{-1} feature to the triply degenerate IR active $\nu_4(T_2)$ bending mode of SO_4^* split by the trigonal distortion of the crystal field (see Table I). Based on the relative intensities of the 637- and 641-cm^{-1} lines constituting the 640-cm^{-1} feature they should be assigned to the ν_4'' and ν_4' modes transformed under the E and A_1 representations of the C_{3v} point group.

The temperature dependences of the the 637- and 641-cm^{-1} lines presented in Fig. 10 reveal that the two modes merge as the temperature grows in. Such a behavior is similar to that found for the ϑ_1 and ϑ_2 stretch modes (see Fig. 8)

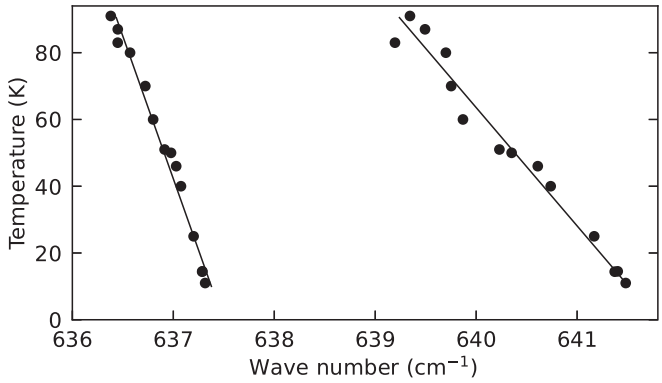

FIG. 10. Frequencies of the 637- and 641-cm^{-1} modes as a function of temperature observed in $CdSO_4$-treated CdTe samples.

whose frequencies coalesce at about 300 K to a value of 1102 cm^{-1} [14,15]. The observed analogy in the temperature behavior of the 640-cm^{-1} feature is also in favor the SO_4^* model.

The model of a trigonally distorted SO_4^* provides a straightforward explanation for such a converging behavior. As described in Sec. III, trigonal distortion of SO_4 trapped in the Cd vacancy implies an orientational degeneracy of the complex with respect to four equivalent ⟨111⟩ directions. We suppose that thermally activated dynamic switching among these equilibrium sites "softens" the distortion and eventually leads to an effective T_d symmetry of the SO_4^* complex, which manifests itself as a convergence of the A_1 and E states into the threefold degenerate T_2.

It remains to discuss the origin of the 517- and 588-cm^{-1} modes seen in Fig. 9. The additional lines which appear in the ^{18}O-enriched sample indicate that both modes are oxygen related. The ν_2 mode of free SO_4^{2-} at 451 cm^{-1} is infrared inactive [25]. Trigonal distortion of SO_4 trapped at the Cd vacancy shifts its frequency down to 418 cm^{-1} and may, in principle, allow its detection by means of infrared absorption (see Table I). On the other hand, our results presented in Sec. IV B imply that the trigonal deformation is not sufficient to result in the infrared activity of the ν_1 mode at 981 cm^{-1}. Moreover, the 517-cm^{-1} line turned out to occur only in very heavily SO_n^*-doped CdTe samples, which might indicate towards formation of another complex consisting of both sulfur and oxygen. At this stage, the bulk of experimental data at our disposal do not allow us to draw unambiguous conclusions on the microscopic origin of the 517- and 588-cm^{-1} modes.

V. SUMMARY

A combined study of sulfur-oxygen complexes in single-crystalline CdTe by IR absorption spectroscopy and first-principles theory was performed. It is shown that the earlier interpretation of the double feature at 1097 and 1108 cm^{-1} as asymmetric stretching vibrations of an SO_2^* molecule has to be revised. Instead, the spectrum of the complex, as obtained from oxygen isotope experiments in the spectral range of symmetric and asymmetric stretching, bending, as well as combinational vibrations, is characteristic for an axially distorted SO_4 tetrahedron. First principles calculations suggest a sulfate ion located on the cation vacancy sites, SO_4–V_{Cd}, as a most plausible model for the complex.

ACKNOWLEDGMENTS

This work was funded by the Deutsche Forschungsgemeinschaft (Grant No. LA 1397/14). V.V.M. acknowledges the support from the Ministry of Education and Science of the Russian Federation. The authors are grateful to the Centre for Information Services and High Performance Computing TU Dresden and the Cyberia Supercomputer Center of Tomsk State University for providing the facilities for high throughput calculations. The authors thanks D. Bastin for help with IR absorption measurements.

[1] L. Verger, J. Bonnefoy, F. Glasser, and P. Ouvrier-Buffet, J. Electron. Mater. **26**, 738 (1997).
[2] T. E. Schlesinger, J. E. Toney, H. Yoon, E. Y. Lee, B. A. Brunett, L. Franks, and R. B. James, Mater. Sci. Eng., R **32**, 103 (2001).
[3] S. Del Sordo, L. Abbene, E. Caroli, A. M. Mancini, A. Zappettini, and P. Ubertini, Sensors **9**, 3491 (2009).
[4] J. M. Burst, J. N. Duenow, D. S. Albin, E. Colegrove, M. O. Reese, J. A. Aguiar, C.-S. Jiang, M. Patel, M. M. Al-Jassim, D. Kuciauskas *et al.*, Nat. Energy **1**, 16015 (2016).
[5] W. Metzger, S. Grover, D. Lu, E. Colegrove, and J. Moseley, C. L. Perkins, X. Li, R. Mallick, W. Zhang, R. Malik, J. Kephart *et al.*, Nat. Energy **4**, 837 (2019).
[6] J. D. Major, Semicond. Sci. Technol. **31**, 093001 (2016).
[7] D. Albin, Y. Yan, and M. Al-Jassim, Prog. Photovoltaics **10**, 309 (2002).
[8] B. A. Korevaar, J. R. Cournoyer, O. Sulima, A. Yakimov, and J. N. Johnson, Prog. Photovoltaics **22**, 1040 (2014).
[9] S. A. Awadalla, A. W. Hunt, K. G. Lynn, H. Glass, C. Szeles, and S.-H. Wei, Phys. Rev. B **69**, 075210 (2004).
[10] M.-H. Du, H. Takenaka, and D. J. Singh, J. Appl. Phys. **104**, 093521 (2008).
[11] A. Klein, J. Phys. Condens. Matter **27**, 134201 (2015).
[12] D. M. Meysing, M. O. Reese, C. W. Warren, A. Abbas, J. M. Burst, H. P. Mahabaduge, W. K. Metzger, J. M. Walls, M. C. Lonergan, T. M. Barnes *et al.*, Sol. Energy Mater. Sol. Cells **157**, 276 (2016).
[13] A. Abbas, D. Meysing, M. Reese, T. Barnes, J. Walls, and C. Wolden, Sol. Energy **159**, 940 (2018).
[14] G. Chen, I. Miotkowski, S. Rodriguez, and A. K. Ramdas, Phys. Rev. Lett. **96**, 035508 (2006).
[15] G. Chen, I. Miotkowski, S. Rodriguez, and A. K. Ramdas, Phys. Rev. B **75**, 125204 (2007).
[16] E. V. Lavrov, D. Bastin, J. Weber, J. Schneider, A. Fauler, and M. Fiederle, Phys. Rev. B **84**, 233201 (2011).
[17] J. T-Thienprasert, T. Watcharatharapong, I. Fongkaew, M. H. Du, D. J. Singh, and S. Limpijumnong, J. Appl. Phys. **115**, 203511 (2014).
[18] P. E. Blöchl, Phys. Rev. B **50**, 17953 (1994).
[19] X. Gonze, F. Jollet, F. Abreu Araujo, D. Adams, B. Amadon, T. Applencourt, C. Audouze, J.-M. Beuken, J. Bieder, A. Bokhanchuk *et al.*, Comput. Phys. Commun. **205**, 106 (2016).

[20] M. Torrent, F. Jollet, F. Bottin, G. Zérah, and X. Gonze, Comput. Mater. Sci. **42**, 337 (2008).

[21] *CdTe Crystal Structure: Datasheet from "PAULING FILE Multinaries Edition—2012"* (Springer-Verlag, Berlin, 2016).

[22] S. Baroni, S. de Gironcoli, A. Dal Corso, and P. Giannozzi, Rev. Mod. Phys. **73**, 515 (2001).

[23] C. Audouze, F. Jollet, M. Torrent, and X. Gonze, Phys. Rev. B **73**, 235101 (2006).

[24] C. Audouze, F. Jollet, M. Torrent, and X. Gonze, Phys. Rev. B **78**, 035105 (2008).

[25] G. Herzberg, *Molecular Spectra and Molecular Structure II. Infrared and Raman Spectra of Polyatomic Molecules* (Van Nostrand, Princeton, 1960).

[26] J. Decius, E. Coker, and G. Brenna, Spectrochim. Acta **19**, 1281 (1963).

[27] E. B. Wilson, J. C. Decius, and P. C. Cross, *Molecular Vibrations* (Dover, New York, 1980).